Optics Communications 285 (2012) 3228–3233

Contents lists available at SciVerse ScienceDirect

Optics Communications

journal homepage: www.elsevier.com/locate/optcom

Two bit all-optical analog-to-digital converter based on nonlinear Kerr effect in 2D photonic crystals

Bahar Youssefi [a], Mohammad Kazem Moravvej-Farshi [a,*], Nosrat Granpayeh [b,1]

[a] Advanced Devices Simulation Lab (ADSL), Faculty of Electrical and Computer Engineering, Tarbiat Modares University (TMU), P.O. Box 14115-194, Tehran 1411713116, Iran
[b] Faculty of Electrical and Computer Engineering, K.N. Toosi University of Technology, P.O. Box 16315-1355,Tehran 1431714191, Iran

ARTICLE INFO

Article history:
Received 27 June 2011
Accepted 24 February 2012
Available online 10 March 2012

Keywords:
All-optical analog to digital converter
Nonlinear Kerr effect
Photonic crystals

ABSTRACT

We have demonstrated the performance of a novel design for a single wavelength 2-bit all-optical analog-to-digital converter (ADC). This converter consists of two high efficient channel drop filters with a coupled cavity-based wavelength selective reflector in a 2D photonic crystal with total length of 15.87 μm. The A/D conversion is achieved by using nonlinear Kerr effect in the cavities. The output ports switch to state '1' at different input power levels to generate unique states preferred for an ADC. This conversion is simulated by the finite difference time domain (FDTD) method for 5 different power levels. The proposed structure can function as a two-bit ADC with a 60 mW/μm input pulse and its maximum sampling rate is found to be ~45 GS/s.

1. Introduction

Using the photonic devices for creation or improvement of analog-to-digital converter (ADC) has been started since 1974. Development of optical technologies has overcome the fundamental limitations of electronic ADCs. The name of photonic ADC is valid for a device with an analog optical signal input and a digital optical signal output. To the best of our knowledge, a few numbers of all-optical ADCs have been proposed, simulated or fabricated. On the other hand, in some literatures the ADCs with analog electrical inputs that use optical devices to convert input to digital are named optical ADCs [1]. Optical ADCs propose better performance and accuracy compared to the electronic ones, because of the existence of ultra-low jitter in optical sources and immunity of the optical signals from electromagnetic interference and noise. Moreover, all-optical ADCs do not require optical-electrical conversion or vice versa. Hence they have higher speed compared to the electronic or optoelectronic ones [1–4].

Several all-optical ADCs have been demonstrated, most of which are based on optical nonlinear effects with one-kilometer long optical fibers [5–7]. The long fiber devices are not suitable for integration [2–7]. An optical ADC based on nonlinear effects in chalcogenide waveguide has recently been reported [8]. Although integrable, this ADC is 6 cm long. Moreover, photonic crystal ADC with oblique coupled defect resonator waveguides has also been designed and fabricated [2,3].

In this paper, we have proposed an integrable all-optical ADC based on nonlinear Kerr effects in pillar photonic crystals (PhCs), whose total length is shorter than 20 μm. The proposed device is capable of supplying five discrete logic states, with an adequate input power.

The rest of the paper is organized as follows. In Section 2, we present the principles of the proposed two-bit all-optical A/D converter. In Section 3, we discuss about the design of ADC parameters. Section 4 is devoted to results and discussions. Finally, the paper is concluded in Section 5.

2. Principles of the proposed two-bit optical A/D converter

The two narrow band channel-drop filters (CDFs) are the key elements in our proposed optical photonic crystal (PhC) ADC. We have used a three port system based on two coupled cavities in both drop and reflector sections. This system can provide a practical approach for obtaining a high efficient CDF with narrow full width at half maximum (FWHM), and no reduction in transmission efficiency. The coupled cavities of the drop and the reflector sections are located at both sides of the bus waveguide to prevent the direct coupling between them, as shown in Fig. 1. It has been shown that the FWHM in a system composed of two identical coupled cavities, made of PhC point defects, is about one half of its value in a system made of similar single point defects, when the phase-difference ($\Delta\phi$) of the lightwave coupling between the cavities is near zero [9]. Also, it has been shown that this phase difference, in the modified hybrid waveguide with two coupled point defects (HW_2) is close to zero for various defect radii [9].

Our proposed ADC is designed and simulated by 2D finite-difference time-domain (FDTD) method; using the effective refractive

* Corresponding author. Tel.: +98 21 82883367; fax: +98 21 82884325.
E-mail addresses: youssefi@ieee.org (B. Youssefi), farshi_k@modares.ac.ir (M.K. Moravvej-Farshi), Granpayeh@eetd.kntu.ac.ir (N. Granpayeh).
[1] Tel.: +98 21 88469465; fax: +98 21 88462066.

0030-4018/$ – see front matter © 2012 Elsevier B.V. All rights reserved.
doi:10.1016/j.optcom.2012.02.081

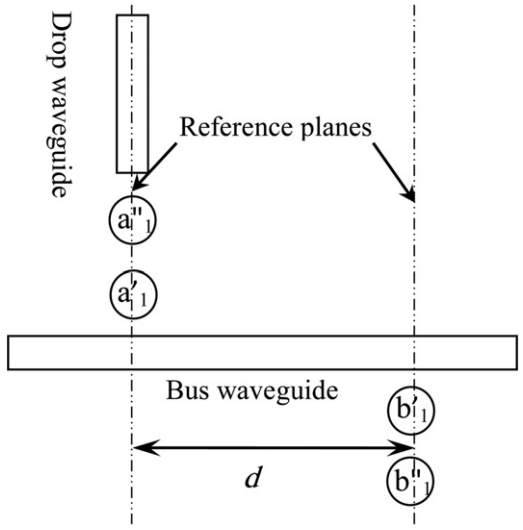

Fig. 1. Schematic view of a three-port CDF with coupled cavities based wavelength selective-reflector.

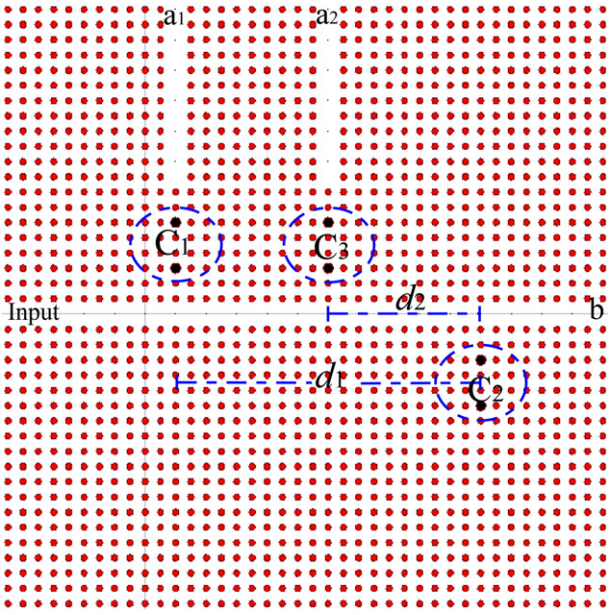

Fig. 2. A Schematic top view of the proposed 2-bit all-optical ADC.

index to approximate the behavior of a 3D structure. To obtain a relation for the drop efficiency, some parameters should be defined. Those are $1/\tau_0$ representing the decay rate due to internal loss of energy, ω_{0a} and ω_{0b} representing the resonance frequencies of the coupled defects in the drop and the reflector cavities, respectively, $1/\tau_1$ denoting the coupling decay rate of cavity a'$_1$ to the bus waveguide, and $1/\tau_2$ representing the total decay rates of the cavity a"$_1$ into the cavity a'$_1$ and vice versa and also the decay rate of the cavity a"$_1$ into the drop waveguide. Considering the structure of Fig. 1 and using the coupled mode theory (CMT), it can be proved that if $\Delta\phi\approx 0$, $\omega_{0a}=\omega_{0b}=\omega_0$ and $\tau_0>>\tau_1$ and τ_2, the drop efficiency at resonance frequency can be expressed as [9]:

$$\eta\Big|_{\omega=\omega_{0a,0b}} = |D|^2\Big|_{\omega=\omega_{0a,0b}} = \frac{8k(1-\cos\phi)}{8k^2(1-\cos\phi)+4k(1-\cos\phi)+1} \tag{1}$$

where $k=\tau_2/\tau_1$ and $\phi=2\beta d$, where β is the propagation constant of the bus waveguide, and d is the distance between two reference planes. It has been demonstrated that for $k=1/4$, if the phase condition $\phi=(2n+1)\pi$ (for either ω_{0a} or ω_{0b} with n being an integer) is satisfied, the channel drop efficiency becomes 100% [9].

Using the coupled mode theory, one can easily show that the condition $k=1/4$ is satisfied for the structure of Fig. 1 [9,10]. Therefore, to obtain the maximum drop efficiency, we should only satisfy the phase condition. Furthermore, assuming $\omega_{0a}\neq\omega_{0b}$ and $\tau_0>>\tau_3$ ($1/\tau_3$ being the decay rate of the cavity a'$_1$ into the bus waveguide) the maximum drop efficiency reduces to [9]:

$$\eta_{\max}\Big|_{\omega_{0a,0b}} = \frac{64}{\tau_1^2(\omega_{0b}-\omega_{0a})^2} = \frac{4}{Q^2(\omega_{0b}/\omega_{0a}-1)^2+4} \tag{2}$$

where Q represents the coupled cavities quality factor. Eq. (2) shows that an increase in either the quality factor or the mismatch between the resonance frequencies, $(\omega_{0b}/\omega_{0a}-1)$, leads to reduction of the maximum drop efficiency. This is very important to be noticed for the proposed ADC. A schematic top view of the proposed 2-bit all-optical ADC is shown in Fig. 2. In this ADC, we have two CDFs with a little difference between the resonant frequencies of the cavities caused by the Kerr effect and different localized power in the cavities.

To realize a 2-bit optical ADC, at least, four discrete logic states are needed, for which at least two drop waveguides are required. The proposed structure has three coupled cavities, C_1, C_3 (drop cavities), and C_2 (reflector cavity), isolated from each other. Each of these coupled cavities, surrounded by a dashed-circle (as shown in Fig. 2) consists of two coupled cavities made of two rods of the same radii (r_d) that act as point defects. The drop waveguides (a_1 and a_2) and the bus waveguide (b) are W1-type that can be made by removing a series of rods in the same row/column. The band diagram for the W1-type PhC waveguide is illustrated in Fig. 3. The dotted–dashed curve shows the propagating mode in the W1 waveguide.

The input optical signal is assumed to be a sinusoidal wave. The resonance frequencies of all three coupled cavities are assumed to be a bit higher than the frequency of the input lightwave. When the power of the incident wave is lower than the threshold, for the Kerr effect to be effective in the cavities, most of the input signal is transmitted to port b. As the power of the input signal reaches the threshold, the Kerr effects in the drop and the reflector cavities cause the resonance frequencies to drop and shift toward the frequency of the input signal. Hence, the output power at ports a_1 and a_2 are increased, whereas the output power at port b is decreased. Considering the variation of these three output ports, we can achieve four discrete states by comparing to an appropriate threshold level. This variation depends on the radii of the defects (r_d), the distances between the reflector cavity (C_3) and the drop cavities ($C_{1,2}$), $d_{1,2}$, as depicted in Fig. 2, the Kerr coefficient in the defects' material, and the power of the input signal. Hence, we have to choose suitable values for these

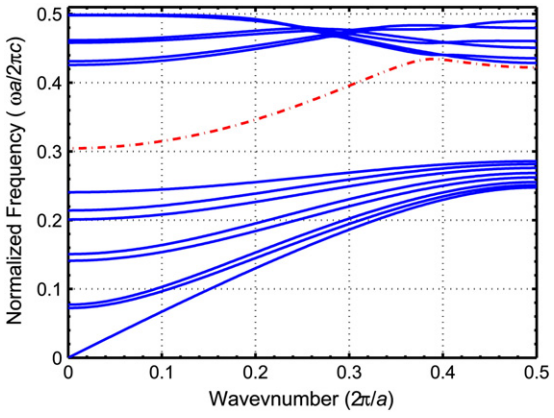

Fig. 3. Dispersion diagram of the W1-type bus waveguide.

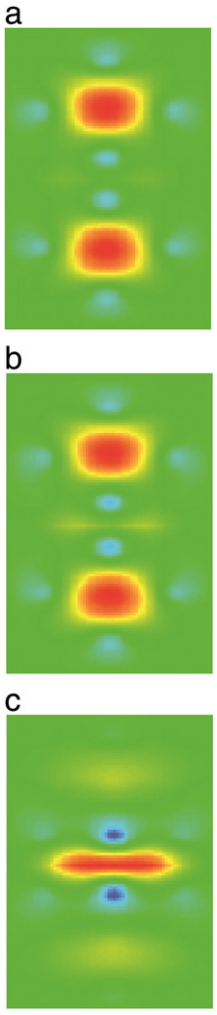

Fig. 4. Electric-field distribution of TM defect states in an array of dielectric rods for coupled defects for various defect sizes. (a) $r_d=0.2a$, (b) $r_d=0.41a$, and (c) $r_d=0.43a$.

parameters according to the procedure explained in the following section.

3. Design of the ADC parameters

Our proposed ADC is designed on a 2D-PhC platform composed of Si rods of radii $r=0.2a$ and refractive index of $n_{Si}=3.4$ arranged with a square lattice of constant $a=530$ nm in an air background. Such pillar PhCs have bandgaps solely in TM polarization. In order to be able to take advantage of the nonlinear Kerr effect at lower input power, we have used doped glass with high Kerr coefficient ($n_2 \sim 10^{-14}$ m^2-w^{-1}), for the point-defects with linear refractive index of $n_0=1.4$ [11,12]. To achieve the maximum drop efficiency in either drop waveguides, the phase condition should be satisfied in that waveguide. For this purpose, all three cavities should be single mode. Although for each isolated point defect single mode condition sustains for $r_d<0.53a$, for the coupled cavities single modes occur for $r_d<0.41a$. Fig. 4 illustrates the electric field distributions in the vicinity of two coupled cavities for three different radii $r_d=0.2a$ (a), $r_d=0.41a$ (b), and $r_d=0.43a$ (c). As seen in Fig. 4(b), at $r_d=0.41a$ modes of two coupled cavities start to overlap. Hence, we varied the defects radii over the range of $0\le r_d\le 0.41a$ by steps of $0.01a$, and calculated the resonance frequencies of the coupled cavities. The numerical results are illustrated in Fig. 5.

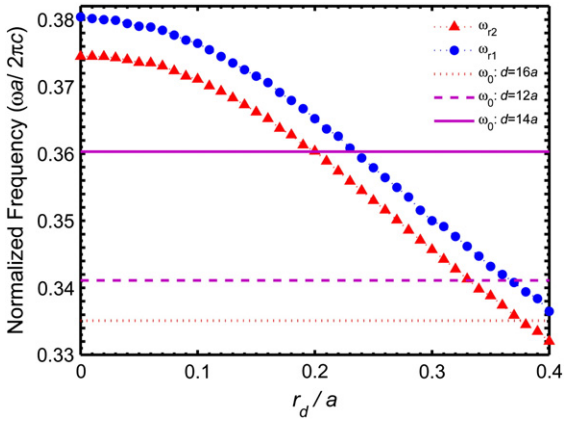

Fig. 5. The resonance frequencies ω_{r1} (circles) and ω_{r2} (triangulars) vesrus r_d/a. Horizontal lines represent ω_o for different lateral separations between C_3 and C_2; i.e., $d_2=12a$ (dashes), $14a$ (solid line), and $16a$ (dots).

Table 1
Three different radii of defects and their parameters.

r_d/a	$\omega_r(2\pi c/a)$	$\omega_o(2\pi c/a)$	$\Delta\omega(2\pi c/a)$	d_1/a	d_2/a
0.41	0.33546	0.33514	3.2×10^{-4}	48	16
0.33	0.34131	0.34110	2.1×10^{-4}	20	12
0.20	0.36037	0.36030	7.0×10^{-5}	42	14

As shown in Fig. 5, each coupled cavity has two resonance frequencies ω_{r1} (triangles) and ω_{r2} (circles). Now by varying the lateral separations d_1 (between the coupled cavities C_1 and C_2) and d_2 (between C_3 and C_2) we watch for the resonance frequencies at which the phase condition is satisfied. For each two coupled cavities (e.g., C_1 and C_3, or C_2 and C_3) to be isolated from each other their

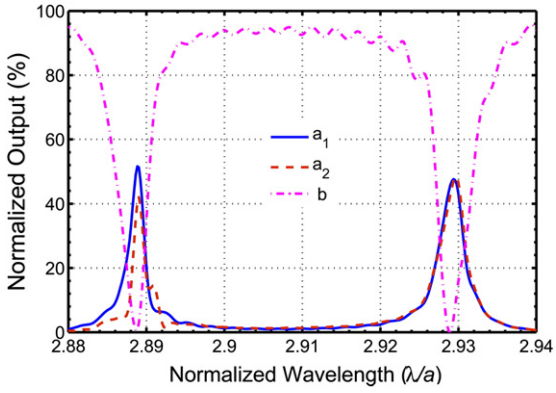

Fig. 6. Transmission spectra of output ports a_1, a_2 and b, for $r_d=0.33a$, $d_1=20a$, and $d_2=12a$.

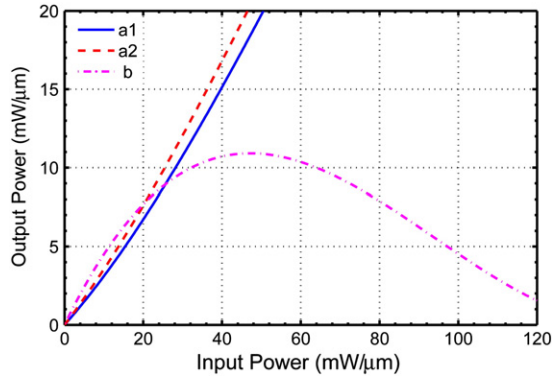

Fig. 7. ADC outputs-input responses for $r_d=0.33a$, $d_1=20a$, and $d_2=12a$.

Table 2
Ratio of the powers of output ports a_2 to a_1 for different distances between reflector and cavity C_2.

d_2	6a	7a	8a	9a	10a	11a	13a	14a
a_2/a_1	%25.7	%72.7	%5.6	%61.5	%35.4	%9.0	%15.9	%16.2

separation should be $d_{1,2} \geq 6a$. Having found the wave vectors at which the phase conditions are satisfied, we extract the corresponding input signal frequencies (ω_0) from Fig. 3. Among these frequencies, we are only interested in those that are a bit smaller than the cavities resonance frequencies. The three horizontal lines, depicted in Fig. 5, represent such frequencies. These three correspond to $d_2 = 12a$, 14a, and 16a, respectively. An appropriate input power can enhance the Kerr effect. This, in turn, shifts ω_r toward ω_0 and hence increases the drop efficiency. For any given d_2 and its corresponding ω_r and β we can find a minimum value of d_1 that can satisfy the phase conditions. Table 1, relates the three values of d_2/a together with their corresponding values of ω_r, ω_0, $\Delta\omega$, r_d/a, and d_1/a. As can be seen from this table, the smallest device size for which the maximum drop efficiency can be achieved is obtained by $r_d/a = 0.33$ for which $d_1 = 20a$, and $d_2 = 12a$.

4. Results and discussions

Fig. 6 illustrates the transmission spectra at ports a_1 (solid curve), a_2 (dashes) and b (dotted-dashes). In the higher wavelengths range, outputs a_1 and a_2 are almost the same, because the conditions for maximum drop efficiency are satisfied for both drop waveguides. Fig. 7 illustrates the output powers at ports a_1, a_2, and b, versus the input power. This figure shows that the present geometry does not provide a threshold level by which one can attain four discrete logic states, required for the two-bit ADC to function. That is due to the fact that the outputs at ports a_1 and a_2 are approximately the same.

Table 3
Input power ranges and their corresponding logic states compared to threshold level of 3.55 mW/μm with %2 margin derived from Fig. 9.

Input power (mW/μm)	a_1	a_2	b
$0 < P_{in} < 10.60$	0	0	0
$11.90 < P_{in} < 13.44$	1	0	1
$13.88 < P_{in} < 15.10$	1	1	1
$16.80 < P_{in} < 18.90$	1	1	0

In order to attain a two-bit ADC, we should change either d_1 or d_2 to perturb the phase condition. However, to keep the device length as short as possible, we keep the longer separation (d_1) constant and vary the shorter one over the range $6a \leq d_2 \leq 14a$. Note that 6a is the minimum separation for which the coupled cavities remain isolated. To find proper separation for which at least four discrete levels are attainable, the differences between the output powers at ports a_1 and a_2 should be examined. Table 2 presents the ratios of the output at port a_2 to that of port a_1 for different values of d_2. When this ratio is too low, the input power required for the output at port a_2 to reach the threshold level becomes too high. On the other hand, when the ratio is too high the output cannot possess the four discrete logic states required for the two-bit ADC. As can be seen from Table 2, values of the ratios (a_2/a_1) for $d_2 = 9a$ and 10a are neither too high nor too low. Hence, we examine the ADC characteristics for these two values of d_2.

Fig. 8 illustrates the transmission spectra for the three output ports (a_1, a_2, and b) of the ADC with $r_d = 0.33a$, $d_1 = 20a$, and $d_2 = 9a$. Fig. 9 shows the corresponding outputs-input responses for

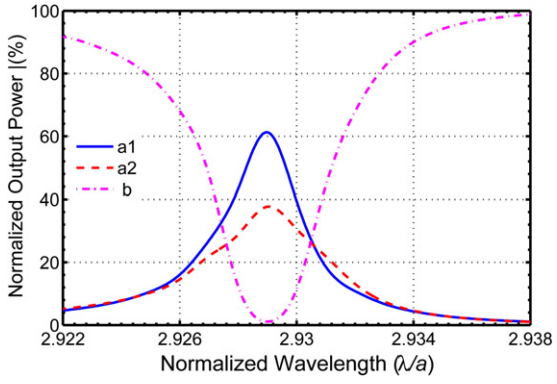

Fig. 8. Transmission spectra of output ports a_1, a_2 and b, for $r_d = 0.33a$, $d_1 = 20a$, and $d_2 = 9a$.

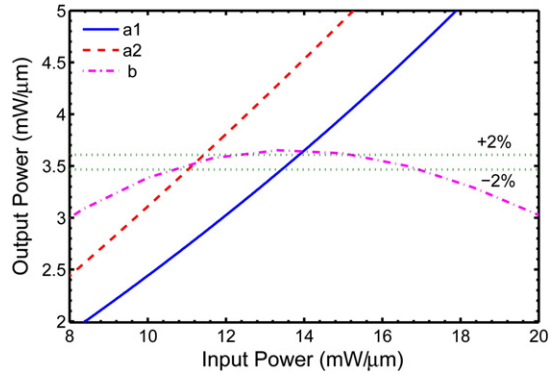

Fig. 9. ADC outputs-input responses for $r_d = 0.33a$, $d_1 = 20a$, and $d_2 = 9a$.

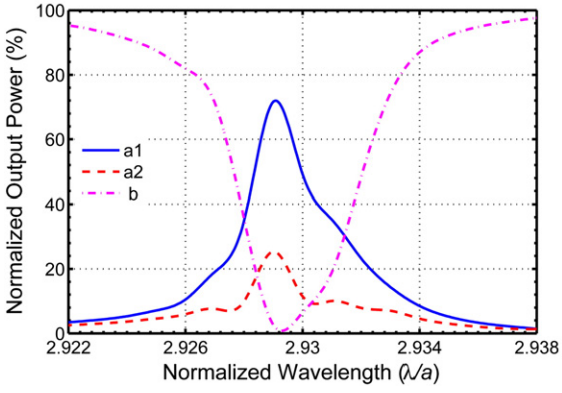

Fig. 10. Transmission spectra of output ports a_1, a_2 and b, for $r_d = 0.33a$, $d_1 = 20a$, and $d_2 = 10a$.

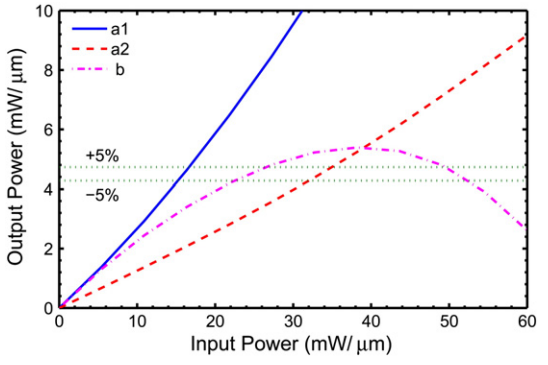

Fig. 11. ADC outputs-input responses for $r_d = 0.33a$, $d_1 = 20a$, and $d_2 = 10a$.

Table 4
Input power ranges and their corresponding logic states compared to the threshold level of 4.5 mW/μm with %5 margin derived from Fig. 10.

Input power (mW/μm)	a_1	a_2	b
$0<P_{in}<14.96$	0	0	0
$16.46<P_{in}<21.22$	1	0	0
$27.17<P_{in}<32.83$	1	0	1
$35.13<P_{in}<49.19$	1	1	1
$51.49<P_{in}<60$	1	1	0

the same ADC. The horizontal lines in this figure indicate the margins of ±%2 about the threshold level. The logic levels are assumed to be "1" when the corresponding output levels are higher than the threshold, and are assumed "0" otherwise. Table 3 shows these four quantized states and their corresponding range of input powers. For this configuration, we have examined the logic levels for the margins

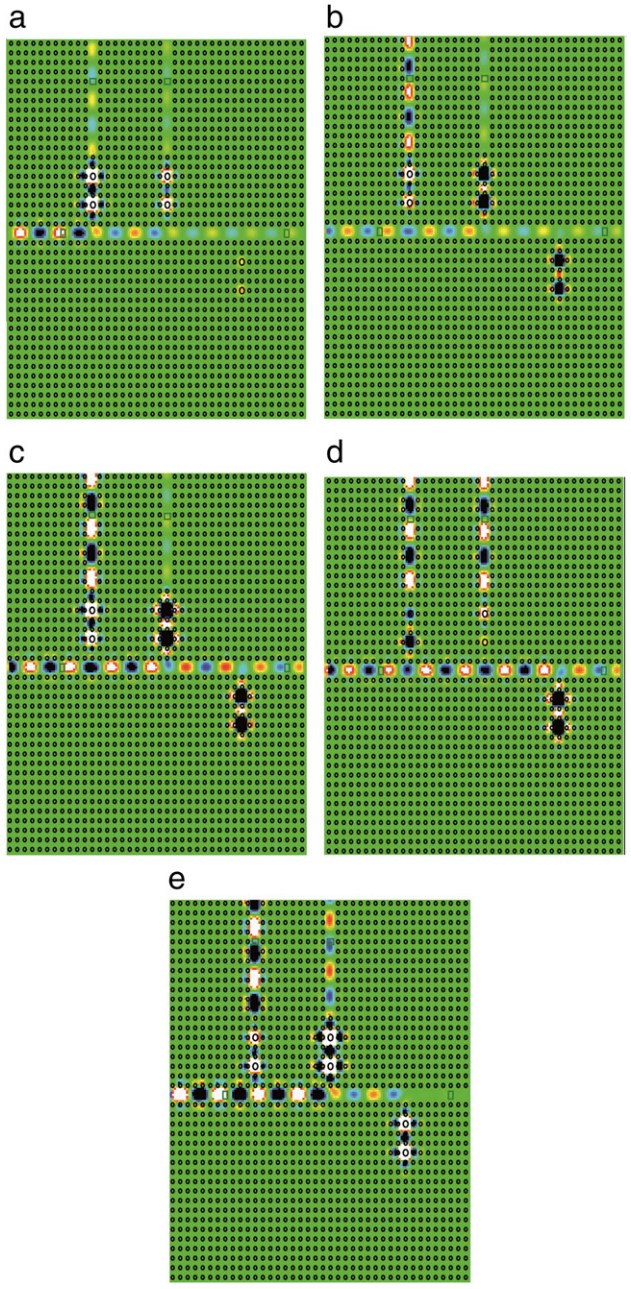

Fig. 12. Field distributions of five logic states for $r_d=0.33a$, $d_1=20a$, and $d_2=10a$ and input power of (a) 3, (b) 20, (c) 28, (d) 45 and (e) 60 (mW/μm).

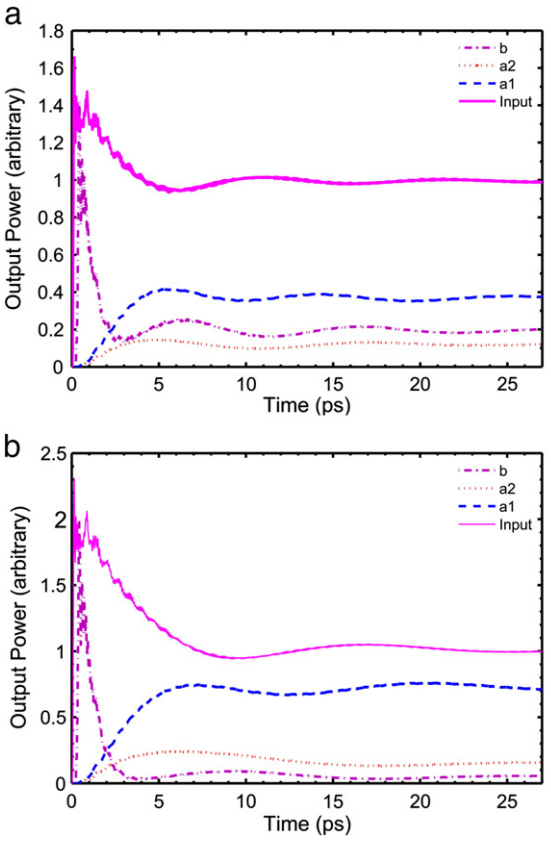

Fig. 13. Time responses of the outputs at ports a_1 (dashes), a_2 (dots), and b (dotted–dashed) for the ADC shown in Fig. 2 with $r_d=0.33a$, $d_1=20a$, and $d_2=10a$ in response to an input step signal of power (a) 6 mW/μm and (b) 60 mW/μm.

higher than ±2% to see whether this configuration could function as a two-bit ADC. However, we have realized that with higher margins the state "101" vanishes and the ADC cannot function as a two-bit converter.

Then, we obtained the transmission spectra and the output–input responses for the ADC with $r_d=0.33a$, $d_1=20a$, $d_2=10a$, and $a_2/a_1=35.4\%$. The respective numerical results are illustrated in Figs. 10 and 11.

Fig. 11 shows that with the threshold level of 4.5 ±%5 mW/μm, the ADC can support five quantized logic states. Table 4 relates these five distinct logic states and the corresponding ranges for the required input power. Distributions of the electric fields at the three output ports in response to five specific input signals of 3, 20, 28, 45, and 60 mW/μm that have created the five discrete logic state of "000," "100," "101," "111," and "110, respectively," are illustrated in Fig. 12, as an example.

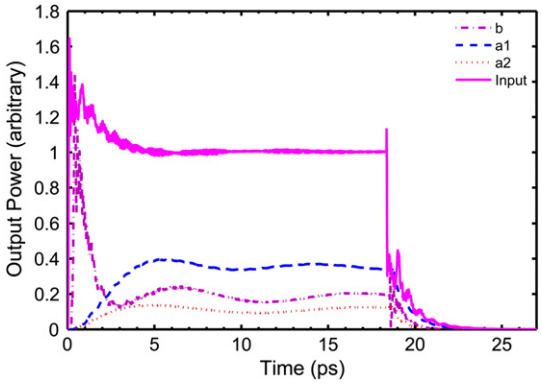

Fig. 14. Time response of the ADC output ports for a step input of 6 mW/μm.

4.1. Time response of the proposed all-optical ADC

Sampling rate of an ADC is one of the most basic properties of the converter. In order to obtain the sampling rate of the proposed all-optical ADC, several step signals of various powers are applied to the input port and the outputs responses are sampled as a function of time. By comparing the numerical results, we have realized that the lower the input power the longer would be the time for the output to become stable. Fig. 13 compares the time responses of the outputs at ports a_1 (dashes), a_2 (dots), and b (dotted-dashes) in response to two input signals (solid curve) of powers 6 (a) and 60 mW/μm (b), as an example. A careful inspection of Fig. 13 (a) shows that the time required for the output signals to reach to 95% of their final values is about 18.3 ps. Similarly, from Fig. 13 (b) one can realize that the outputs take about 12.7 ps to become stable. Simulations show that 18.3 ps is the maximum response time for the proposed ADC to have stable outputs even for lower input powers. Hence, for proper function of the proposed ADC, in response to a pulse-chain, minimum widths of these pulses should be 18.3 ps.

Since the maximum sampling rate is determined by minimum period of the input pulse, we need to calculate the ADC time response for the output signals in response to the sudden fall of the input pulse. Fig. 14 compares outputs in response to an input pulse of width 18.3 ps and power of 6 mW/μm. As can be seen from this figure, all three output signals vanish 3.93 ps after the input signal is in its off state. This means that the minimum period of the input pulse is about 22.23 ps which leads to the maximum possible sampling rate of 45 GS/s.

5. Conclusion

In this paper, we have proposed an all-optical 2-bit analog-to-digital converter (ADC) and have demonstrated its performance. To do this, we used a highly efficient channel drop filter with wavelength-selective reflection feedback. To detain narrow FWHM, the coupled defects were used as drop and reflector cavities instead of the single ones. The distances between the reflector cavity and drop cavities were accurately selected, such that the drop efficiency of one cavity to be %35.4 of that of the other. Therefore by using a material with high Kerr coefficient, the structure could support five discrete logic states at different input power levels. The responses of the ADC were simulated by using the 2D-FDTD method. Simulations show that the required input power to attain these five discrete states is 60 mW/μm and the maximum possible sampling rate is ~45 GS/s.

References

[1] G.C. Valley, Optics Express 15 (2007) 1955.
[2] B. Miao, C. Chen, A. Sharkway, S. Shi, D.W. Prather, Optics Express 14 (2006) 7966.
[3] A. Sharkawy, C. Chen, B. Miao, S. Shi, D. Prather, Proceedings of SPIE 7348 (2009) 1.
[4] S. Yu, S. Koo, X. Piao, N. Park, Application of slow-light photonic crystal structures for ultra-high speed all-optical analog-to-digital conversion, Microoptics Group (OSJ/JSAP, 2009.
[5] T. Nishitani, T. Konishi, K. Itoh, IEEE Journal of Selected Topics in Quantum Electronics 14 (2008) 724.
[6] Y. Miyoshi, S. Takagi, S. Namiki, K.-I. Kitayama, IEEE Journal of Lightwave Technology 28 (2010) 415.
[7] T. Konishi, H. Goto, T. Kato, K. Kawanishi, All optical analog-to digital conversion: principle and recent progress, IEEE, APCC, 2009, p. 487.
[8] R. Pant, C. Xiong, S. Madden, B.L. Davies, J. Eggleton, B., Optics Communication 283 (2010) 2258.
[9] K. Fasihi, S. Mohammadnejad, Optics Express 17 (2009) 8983.
[10] H. Ren, C. Jiang, W. Hu, M. Gao, J. Wang, Optics Express 14 (2006) 2446.
[11] M.A. Mansouri-Birjandi, M.K. Moravvej-Farshi, A. Rostami, Applied Optics 47 (2008) 5041.
[12] E.A. Saleh, M.C. Teich, Fundamental of photonics, John Wiley & Sons, 1991, p. 732.